Signal Deformation Monitoring for Dual-Frequency WAAS

R. Eric Phelts, Gabriel Wong, Todd Walter, and Per Enge, *Stanford University*

BIOGRAPHY

R. Eric Phelts, Ph.D., is a research engineer in the Department of Aeronautics and Astronautics at Stanford University. He received his B.S. in Mechanical Engineering from Georgia Institute of Technology in 1995, and his M.S. and Ph.D. in Mechanical Engineering from Stanford University in 1997 and 2001, respectively. His research involves signal deformation monitoring techniques and analysis for SBAS and GBAS.

Gabriel Wong is an Electrical Engineering Ph.D. candidate at the Stanford University GNSS Research Laboratory. He has previously received an M.S.(EE) from Stanford University, and a B.S.(EECS) from UC Berkeley. His current research involves signal deformation monitoring and mitigation for GNSS signals.

Todd Walter, Ph.D., is a senior research engineer in the Department of Aeronautics and Astronautics at Stanford University. Dr. Walter received his Ph.D. from Stanford and is currently working on modernization of the Wide Area Augmentation System (WAAS) and defining future architectures to provide aircraft guidance. Key contributions include early prototype development proving the feasibility of WAAS, significant contribution to the WAAS MOPS, design of ionospheric algorithms for WAAS, and development of dual frequency algorithms for SBAS. He is a fellow of the Institute of Navigation and serves as its president.

Per Enge, Ph.D., is a professor of aeronautics and astronautics at Stanford University, where he is the Kleiner-Perkins Professor in the School of Engineering. He directs the GNSS Research Laboratory, which develops satellite navigation systems. He has been involved in the development of the Federal Aviation Administration's GPS Wide Area Augmentation System (WAAS) and Local Area Augmentation System (LAAS). For this work, Enge has received the Kepler, Thurlow, and Burka awards from the Institute of Navigation (ION). He received his Ph.D. from the University of Illinois. He is a member of the National Academy of Engineering and a Fellow of the IEEE and the ION

ABSTRACT

Previous signal deformation analyses and monitor designs have primarily focused only on threats to the L1 C/A code. They have traditionally relied on a combination of empirical measurements and analytical models of the threats and the user receivers. In the future however, to mitigate ionospheric errors, WAAS will leverage the L5 signal in addition to L1. This means both signals will need to be monitored. While many familiar C/A code signal deformation monitor analyses can be extended and applied to the L5 codes, the monitor needs to be far more sensitive since the dual-frequency combination designed to remove ionospheric errors will amplify any range biases on the signal. At the same time, this correction will drive the range error limits to be smaller. In addition, the new signal deformation monitor needs to detect potential faults on the L5 signal—a something the current design is not easily adapted to do.

In this paper, background is provided on the current WAAS signal deformation monitor along with key measures of its accompanying performance analysis. In addition, the existing L1 fault threat analyses and user constraints are applied to L5 codes and future receivers. Measured data from a dual-frequency prototype signal deformation monitor receiver are then used to infer a reasonable noise model to compare current and proposed monitor designs. From this data, a new signal deformation fault detection algorithm is analyzed and applied to the case of dual-frequency users to determine its performance, relative to the current system. Finally, the results are used to make recommendations on constraints on dual-frequency user receiver configurations. It is believed that the monitor design approach used here may be readily extended for signal deformation monitoring of other GNSS signals of various code modulations.

INTRODUCTION

Signal deformations arise from hardware imperfections or faults in the signal generation hardware on GNSS satellites. When the received signals differ from each other, biases and, subsequently, position errors may

result. High-integrity augmentation systems such as space-base and ground-based augmentation systems (SBAS and GBAS) employ signal deformation monitors (SDM) to measure the received signals and attempt to ensure these errors remain acceptably small for a set of allowed avionics receiver configurations. In all, an effective SDM design will accomplishes the following tow things:

1) Quickly detect anomalous deformations should they arise in the presence of noise and multipath before they cause harm to the user, and
2) Ensure any undetected nominal or faulted signal deformations do not result in unacceptably large range errors.

For aviation users of GPS L1, GBAS and SBAS have developed signal deformation monitoring techniques for just this purpose [1], [2]. After accounting for environmental noise, multipath, and nominal signal deformation biases, multiple monitor receivers compute linear combinations of the outputs from each correlator on the correlation peak. The result is one or more detection metrics that are well-suited for L1 signals, but which may require significant modification to be adaptable to other signals, such as L5. This is of particular concern for WAAS, which proposes to provide integrity for dual-frequency users in the future. The signal deformation bias errors for these users are magnified by the dual-frequency combination, which is necessary to remove ionospheric errors. In this case, the detection performance of the existing algorithm may not be satisfactory even for the L1 signal. And, for L5, none exists.

It follows that to improve SDM performance, one must either significantly reduce the errors users experience due to the faults or improve the monitor to detect more faults. And both of these approaches must take into consideration the L5 signal, which will have very different characteristics and constraints than does L1.

Reducing User Error

Ideally, the user range errors can be reduced by simply limiting the allowed receiver designs to those closest to the reference receiver configuration. In the best case, all receivers would match WAAS reference receiver, making all deformation errors essentially cancel out with the differential correction. While desirable, this is generally impractical since the user receiver designs often cannot be changed at will. Indeed, for L1-only users, the user receiver designs were fixed well before the signal deformation threat was even defined.

For dual-frequency users this constraint may be more easily imposed since the reverse is true—the threat is defined and understood well in advance of the existence of any L5-capable avionics receivers. However, it is still not guaranteed. For this reason, this paper assumes the most of the current MOPS-defined receiver configurations will also be permitted for dual-frequency users; it excludes only double-delta tracking on L1. It further assumes a relatively broad region will be permitted for tracking the L5 signal as well.

Improving Fault Detection Performance

Assuming limited control over the receiver designs dual-frequency WAAS users implement, fault detection must be improved to achieve better SDM performance. This can be accomplished by one or more of the following:

- Wider monitor receiver bandwidth
- Reduced noise thresholds
- Improved detection metric design

Monitor receivers with wide pre-correlation bandwidths filter out less distortion than one with a narrower filter bandwidth. This makes anomalous oscillations and asymmetries more detectable for a given SDM architecture. The drawback is that it potentially leads to larger errors if that bandwidth causes the differential range correction to be less correlated with those errors.

Reduced noise thresholds imply better noise performance due to either additional averaging or to better siting of the antenna. This too would make the monitor more sensitive. Still, the antenna sites and numbers of receivers in WAAS (and many other systems) are fixed and unlikely to change.

Effective metric designs attempt to maximize detection sensitivity by estimating the distortion in the presence of the noise in an optimized way. This is the approach used in [3]; it is the method currently used in the WAAS. In general, this is a preferred approach since it is the most adaptable and amenable to changes in hardware and/or signals.

BACKGROUND: Single-frequency SDM

ICAO Threat Model

Signal deformation threats are defined by the International Civil Aviation Organization (ICAO) Threat Model [4]. They model the types of correlation peak distortion of concern to aviation users. These include distortions, false peaks, and deadzones. Traditionally, augmentation systems have developed ground-based monitors equipped with multi-correlator receivers to quickly detect when a received correlation peak is sufficiently distorted by one or more of these threats [2].

The ICAO Threat model uses three parameters to describe a combination of analog and digital fault modes with three parameters. A second-order step model describes the analog fault modes using two parameters—f_d and σ, which determine the oscillation frequency and the damping, respectively. The digital fault mode is described by a single parameter, Δ, which determines the amount of advance (lead) or delay (lag) of the falling edge of each chip transition. A full description of these equations is provided in [2] and (more concisely) in [5]. Each of these parameters is illustrated in Figure 1, and the parameter ranges are provided in Table 1.

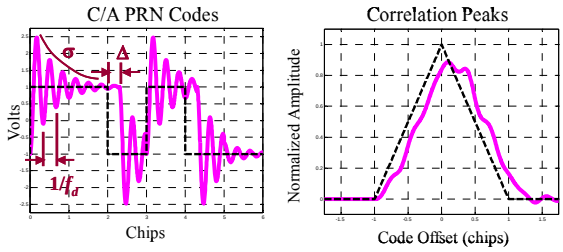

Figure 1. Combination of Analog (Fd and σ) and Digital (Δ) Failure Modes (Ideal <dashed> and Evil <solid> Waveforms Shown.)

Table 1. Signal deformation threat model parameters

	f_d (Mhz)	σ (MNepers/sec)	Δ (ns)
Threat Case A (Digital Fault Only)	N/A	N/A	$10 \le \Delta \le 120$, $-10 \ge \Delta \ge -120$
Threat Case B (Analog Fault Only)	$4 \le f_d \le 17$	$0.8 \le \sigma \le 8.8$	0
Threat Case C (Analog + Digital Fault)	$7.3 \le f_d \le 13$	$0.8 \le \sigma \le 8.8$	$10 \le \Delta \le 120$, $-10 \ge \Delta \ge -120$

Dual-frequency Ionospheric Correction

Currently single frequency users have only a single pseudorange signal, ρ_{L1}, that requires monitoring. Dual frequency users will use a different pseudorange, ρ_{DF}, that incorporates information from a second ranging signal on L5, ρ_{L5}. The dual-frequency pseudorange is modified according to the equation below.

$$\rho_{DF} = 2.26\rho_{L1} - 1.26\rho_{L5} \qquad (1)$$

The dual-frequency combination of Equation 1 eliminates the ionospheric errors—the largest error source for GPS. It permits the WAAS range error limits, or UDREs, to be much smaller and aims to significantly increase availability for those users. However this combination equation also amplifies any biases present on the L1 signal by a factor of 2.26; it scales any biases present on the L5 signal by a factor of 1.26. This means any signal deformation biases that occur on either signal will be significantly larger than they are for users of L1 only. This scaling, in combination with the smaller error limits, makes mitigating signal deformations for dual-frequency WAAS users significantly mode challenging than it is for single-frequency users.

Signal Deformation Monitor for L1-only Users

The current WAAS signal deformation monitor (and reference receiver) is a NovAtel G-II. It has an 18MHz bandwidth and uses an early-minus-late (EML) discriminator with 0.1-chip spacing. Figure 2 shows the configuration of this receiver relative to the L1-only avionics receivers allowed by the MOPS DO-229D [6].

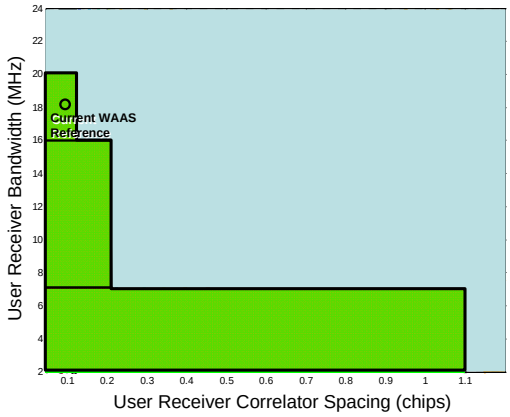

Figure 2. Early-minus-Late receiver configurations allowed by the Minimum Operational Performance Standard (MOPS) DO-229D. The current WAAS reference receiver (NovAtel G-II) has bandwidth of 18MHz and an early-minus-late discriminator with 0.1-chip spacing.

The G-II provides 9 correlator outputs on each channel that are used to measure the symmetry of the correlation peak. Each of the correlators are positioned at offsets relative to an ideal peak ranging from -0.1023 chips to +0.1023 chips, at 0.025-chip intervals. Figure 3 gives an illustration of this configuration.

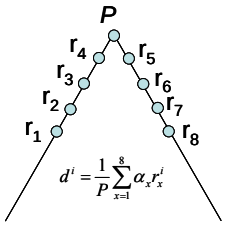

Figure 3. Illustration of correlator outputs on an ideal correlation peak and the computation of a single, normalized detection metric, d^i.

The current WAAS detection metric is simply a linear combination of those correlator outputs according to

$$d^i = \frac{1}{P}\sum_{x=1}^{8} \alpha_x r_x^i \ . \qquad (2)$$

In the above equation, P is the prompt correlator (at an offset of 0 chips) and α_x is a constant. Finally, the detection metric is referenced to the nominal, undistorted signal according to

$$D^i = \frac{\left| d^i - \underset{i}{\text{median}}\left(d^i\right) \right|}{\text{Threshold}} \ . \qquad (3)$$

In the above equation, the nominal metric is represented as the median of that metric across all SVs in view. In modeling analyses, however, the nominal is simply the filtered, undistorted signal.

Note that the current WAAS SDM algorithm is actually the maximum over four such metrics—each with a different set of 8 α_x constants tuned to detect different parts of the threat model. For simplicity, it is equivalent to state that, when maximized, these four metrics acts a single effective threshold-normalized detection metric which thereby determines the ultimate detection performance for the monitor.

DUAL-FREQUENCY SDM

Threat Model

The ICAO threat model used for L1 C/A code is also used to model deformation of the L5 signal. The code on L5 has a chipping rate 10 times as fast and its nominal chip duration is 10 times as short. It is straightforward to apply the threat model transformations to these codes as in [5]. The shortened chip duration implies that the analog fault oscillations on L5 chips appear at one-tenth the frequency they do on C/A chips. And digital faults on the L5 chips appear to be 10 times as large as they do on the C/A code.

There are three separate fault cases which must be mitigated for L5 users. These are as follows:

1) A fault occurs on L1 only
2) A fault occurs on L5 only
3) A fault occurs on L1 and L5 simultaneously

Again, in each of the above cases, the maximum user errors associated with the fault are scaled according to the dual-frequency combination factors associated with each signal. The third, dual-frequency, case was conservatively modeled as having two independent, worst-case faults occur at the same time—one on each signal. Further, the magnitudes of the maximum user errors on each signal were summed, not subtracted, as Equation 1 suggests. While this is likely an overly-pessimistic threat assumption, it helps us to compute an upper bound on the performance of any proposed dual-frequency SDM mitigation strategy.

User Receiver Configurations

The Minimum Operational Performance Standard (MOPS) version DO-229D describes the allowed receiver configuration for L1-only aviation users of WAAS [6]. These include constraints on discriminator type, correlator spacing, bandwidth, and pre-correlation filter differential group-delay. Similar constraints for dual-frequency users have not as yet been defined, but it is anticipated that the design space for these receivers will be far more limited, in order to reduce the magnitude of the potential errors due to signal distortions. However, for the analyses in this paper, the constraints were assumed to be more akin to those of current WAAS receivers. Accordingly, the errors resulting from this analysis should be considered pessimistic. The constraints for the receivers modeled in this paper are listed in Table 2 below.

Table 2. User Receiver Constraints Assumed for the SDM Modeling Analysis

Signal Tracking Capability	L1-Only	Dual-Frequency
Discriminator Type	Early-minus-Late (EML), Double-delta (ΔΔ)	L1: Early-minus-Late L5: Early-minus-Late
Correlator Spacing	EML: 0.045-1.2 chips (max) ΔΔ: 0.045-0.3 chips (max) (Varies with bandwidth constraint as described in [6])	L1: Same as L1-only L5: 0.045-1.2 chips
Bandwidth (MHz)	EML: 2-20MHz ΔΔ: 2-16MHz (Varies with correlator spacing constraint as described in [6])	L1: Same as L1-only L5: 16-24MHz
Group Delay (ns)	0-600ns (Varies with bandwidth constraint as described in [6])	L1: 0-600ns (Varies with bandwidth constraint [6]) L5: 0-150ns

SDM for Dual-Frequency Users

WAAS will soon upgrade to new, NovAtel G-III receivers that will be capable of tracking the L5 signal. These receivers will also have a wider (24MHz) bandwidth, use an EML discriminator with 0.1-chip spacing, and output eight "bin" measurements based on the code chip shape, as opposed to the traditional correlator measurements output by the G-II [7]. Each of these new capabilities can be useful for improving WAAS SDM for dual-frequency users.

The wider bandwidth of the G-III will permit the signal distortion be more observable to the monitor. Still, note from Figure 4 that this bandwidth change moves the reference further away from the set of allowed user receivers. This shift generally leads to larger errors, making prompt detection (i.e., within the 6-second time to-alert requirement) more difficult.

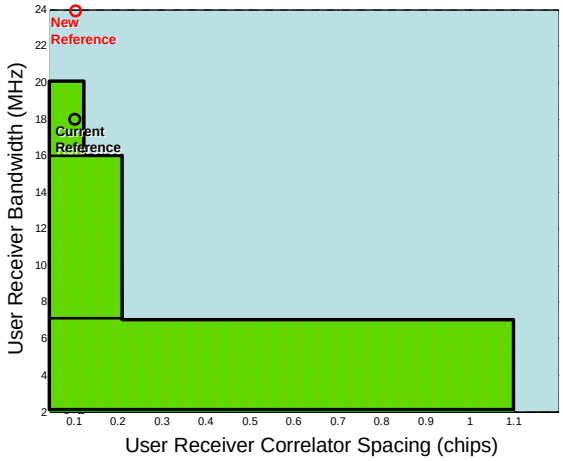

Figure 4. Early-minus-Late receiver configurations allowed by the Minimum Operational Performance Standard (MOPS) DO-229D. The current WAAS reference receiver (NovAtel G-II) and the new reference receiver (NovAtel G-III) configurations are indicated. Both use 0.1-chip EML discriminators, but the G-III has a bandwidth 4MHz wider than the G-II.

The chip-shape based outputs allow processing the distortions pre-correlation, thereby removing one additional filtering step in the process. That step, namely the correlation process itself, typically acts to reduce the amount of distortion that can be observed by the monitor. Combined with the wider bandwidth, these pre-correlation, chip shape outputs can form a powerful tool for signal deformation monitoring.

The chip-based outputs have the added benefit of being less dependent on the code modulation of interest. Figure 5 shows actual high-resolution measurements of 32 GPS PRN codes and overlay one of the L5 codes measured on SVN62 [8]. (For clarity, 5 consecutive positive chips of the L5 signal are plotted.) It is readily observed that the codes shapes look quite similar at the chip transitions. Note that this presents promise not only for signal deformation monitoring of L1 and L5, but perhaps for other code modulations as well.

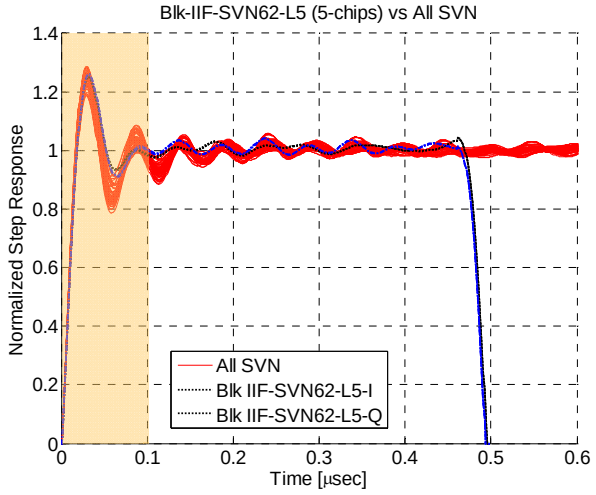

Figure 5. Measurements of C/A codes chips from 32 GPS SVs (red) and a five consecutive L5 code chips (blue) from SVN62. [8]

Figure 6 shows sample outputs from a NovAtel OEMV3 receiver—a receiver quite similar to the future WAAS G-III. (This is the receiver used for the analysis in this paper.) Observe that the actual L1 and L5 chip transitions coincide exactly. It follows that any detection method that acts on the code chip transitions for one code modulation should be relatively easily adapted to the other modulations as well. Figures 7 and 8 illustrate how chip shape outputs are modeled for SDM analyses on both L1 and L5 codes, respectively.

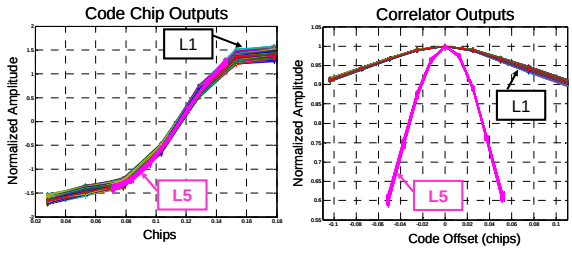

Figure 6. Live measurements of the chip shape outputs and the corresponding correlator outputs from PRN25. (Data taken with a NovAtel OEM-V3.)

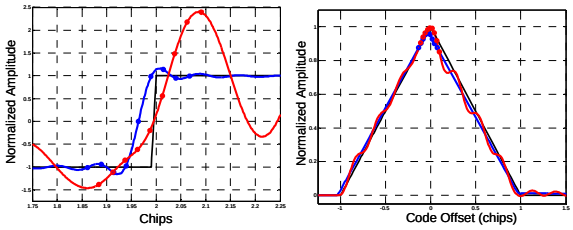

Figure 7. Distorted (red) and nominal (blue) models of chip shape outputs and correlation peak outputs for L1. Analog threat shown (fd=4MHz, σ=0.8MNepers/sec).

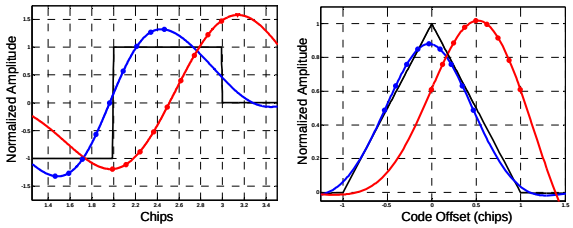

Figure 8. Distorted (red) and nominal (blue) models of chip shape outputs and correlation peak outputs for L5. Analog threat shown (fd=4MHz, σ=0.8MNepers/sec).

The chip-based metrics evaluated in this paper are very straightforward. They are simply differences between the normalized amplitudes of the individual measurements relative to the nominal signal. (See Figure 9 below.) Each individual measurement is simply

$$d_x^i = \frac{1}{P'} b_x \,. \tag{4}$$

In the above equation, $P' = \kappa P$, where P is the prompt measurement from the traditional correlation peak (in Eq. 2) and κ is a scaling constant used to normalize the nominal chip measurements to values between ±1. Given a detection threshold at each bin offset, x, each of the individual detection metrics is then found according to

$$D_x^i = \frac{\left| d_x^i - \underset{i}{\text{median}}\left(d_x^i\right) \right|}{\mathrm{T_x}} \,. \tag{5}$$

The final metric is then the maximum over all 8 individual threshold-normalized metrics.

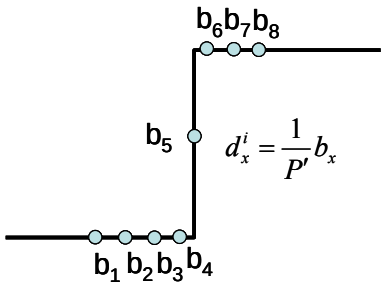

Figure 9. Illustration of chip shape bin outputs on an ideal chip transition and the computation of a single, normalized chip (amplitude) based detection metric, d^i_x, where x ranges from 1 to 8.

In this paper, to compare the detection approaches using a common reference, the NovAtel OEM-V3 was used to approximate the outputs from a WAAS G-III receiver and compute common thresholds. The G-III is not yet fielded and is still unavailable, but the OEM-V3 behaves similarly to the G-III. It is L5-capable, has a 24MHz bandwidth, and it produces chip-shape bin outputs. It can also produce traditional correlation peaks.

There are some small differences however. For one, the OEM-V3 uses NovAtel's proprietary PAC tracking technique instead of narrow correlator (0.1-chip EML on L1); they both use wide correlator tracking for L5 (1.0 chip EML on L5). However, this should have little effect for the analysis of this paper, which does not rely on this data to model the differential correction. Also, this analysis uses very conservative noise estimates, so any potential advantage offered by the PAC technology under nominal environmental/multipath conditions is negated.

Another difference is that the OEM-V3 has slightly different correlator locations than will the G-III, and it has one less bin output and correlator output on the late side (i.e., right side) of the correlation peak. The G-III will have 8 bins, and can produce 9 correlator outputs while the OEM-V3 has only 7 bins, leading to 8 correlator outputs. (Refer to Figure 6.) Again, the effect on the results here should be minor, since all the bin and correlator locations required are still quite close to those of the G-III. The models approximate the true G-III tracking and correlator characteristics more precisely (e.g., Figures 7 and 8), and the noise estimates were, again, worse (higher) than those used in WAAS.

ANALYSIS

All of the inputs needed to analyze the relative performance have been identified in the preceding sections. Given the threat model, Equations 3 and 5 can be used to generate the maximum, steady-state monitor

responses to each threat. The threat model combined with the user receiver design constraints of Table 2 can be used to model the maximum, steady-state user range errors corresponding to each monitor response. Using the OEM-V3, thresholds for each bin can be determined. The correlation peaks can then be computed along with the current WAAS metrics to generate detection thresholds for those as well. Finally, each of the detection methods can then be directly compared to each other to determine their relative performance.

This relative measure is insufficient, however, to fully assess the performance of a proposed monitor design. The monitor must mitigate the hazardous signal deformation faults within the 6-second time-to-alert requirement for all desired error limits. To this end, it is helpful to compute the error limits as a function of the monitor response.

Time-to-Alert Analysis: Time-varying MERR

Once the monitor metrics *m* are designed and the appropriate threshold estimates are applied to them the next step is to analyze the ability of these metrics to detect hazardous faults within the time-to-alert. In other words the monitor must mitigate the threats before they reach the user error limit and lead to hazardously misleading information (HMI). For WAAS SDM, this error limit is also referred to as the Maximum ERror in Range, or MERR.

Table 3. "Static" MERR Error Limits for L1-Only and Dual-frequency Users

UDRE Index (UDREI)	UDRE	MERR for L1-only Users	MERR for Dual-frequency Users
0	0.75	5.01	1.21
1	1	5.12	1.62
2	1.25	5.27	2.03
3	1.75	5.63	2.83
4	2.25	6.08	3.64
5	2.0	6.87	4.86
6	3.75	7.78	6.08
7	4.5	8.76	7.29
8	5.25	9.80	8.51
9	6.0	10.87	9.72
10	7.5	13.09	12.15
11	15	24.78	24.30
12	50	81.15	81.00
13	150	243.06	243.01

The "static" (i.e., time-invariant) MERR is a function of the UDRE. This error limit can be met simply by ensuring the maximum user range error from any undetected signal deformations remain below it. This quantity is defined for L1-only and dual-frequency users according to the table below. Note that when the UDRE index (UDREI) is small, the static error limits are significantly larger for L1-only users than it is for dual-frequency users. This is because the error limits for L1-only users include terms to account for ionospheric errors. (See Table 3.)

An effective signal deformation monitor, however, must detect the deformations promptly, before they cause harm for the users. Accordingly they must take into account the following two additional considerations:

1) No HMI should occur during the transient response between fault onset and steady-state for both user range error, *E*, and monitor metric, *m*.
2) There should be adequate margin between the maximum steady-state user range error and the "static" MERR of Table 3.

A time-varying MERR analysis was developed to address both of these concerns [9].

A detailed derivation of the time-varying MERR formulation explaining how it integrates the time and margin information into a single pass-fail test for meeting the current fault tree allocation for these faults is provided in Appendix A. The sections below describe the inputs and assumptions used to get the results presented in this paper.

MERR Analysis Inputs

The transient responses for SDM are dominated by the responses of the user carrier smoothing filter and smoothing filter used to average the monitor measurements. The time constants for the user smoothing filter and the monitor metric filters are 100 seconds and 50 seconds, respectively. (The user smoothing filter time constant is recommended by MOPS-229D [5].)

The constants, K_{ffd} and K_{md} derive from the false-alarm (P_{fa}) and missed detection probabilities (Pmd), respectively. P_{fa} comes from the current continuity requirement and targets one false alarm per satellite per year; this results in a P_{fa} of 3.2×10-8/SV. It should be noted that this is a conservative value, since the SQM test statistics are highly correlated (over 50 to 100 seconds) and this value assumes independent exposures to false alarm for each second. When expressed in terms of a sigma multiplier for a normal, zero mean probability distribution, the threshold for PFA = 3×10-8 yields a K_{ffd} of 5.54. For a P_{md} of 10-4, K_{md} equals, at most, 4.46. For this analysis the undetected fault allocation, Pa = 6.45×10-10/hr was assumed. The fault prior (P_f) used was 6*1.07×10-5 faults per SV, per hour.

Steady-state User and Monitor Responses

Using the equations outlined in Appendix A and the inputs outlined in the previous section, a MERR "bound" can be found at each desired WAAS error limit (or UDRE) by determining the max E_{ss}, the steady-state user range error (given the discretized ICAO threat model) that corresponds to a given m_{ss}, the maximum steady-state monitor metric value. The horizontal axis is the maximum Threshold-normalized detection metric, $m_{ss}=m/T$ (where, for the current WAAS system, m_{ss} is the final, median-adjusted detection metric as discussed [10]). The threshold is the sum of K_{ffd} multiplied by the (maximum) monitor noise constant σ_{mon}. (Refer to Table 5.7.4.3.1-1.)

A plot of E_{ss} vs. m_{ss} for L1-only WAAS users at a UDRE of 150m (UDREI=13) is given in Figure 10. It corresponds to the case where there the current WAAS reference receiver (G-II) differential correction is applied. The user receiver filters include all the generalized filters allowed by the MOPS DO-229D (as illustrated in Figure 4) [6]. Each point in the plot corresponds to a different threat in the threat model. The blue line provides an upper bound on the error as a function of the minimum monitor response.

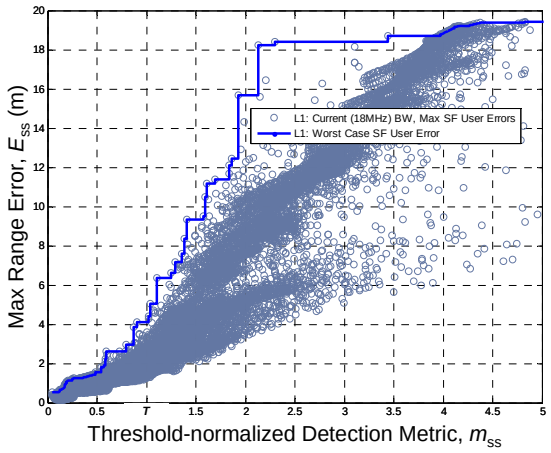

Figure 10. E_{ss} vs. m_{ss} for the current WAAS system for L1-only users. (Reference 18MHz, 0.1 chip).

The procedure for determining the time-varying MERR bound that takes these inputs into account, accounts for margin, and plots the smallest error bound as a function of monitor response, m_{ss} as is as follows:

Procedure:

1) For a given time-varying metric, m, Find $P_{md}(m(t))$ using assumed noise statistics (i.e., σ_{mon}) about $m(t)$ at each time in the step response (given by Eq. A-13) evaluated at the threshold.

In other words, solve

$$P_{md}\left(m(t)\right)=\left(\Phi^{R}\right)\left(K_{ffd}-m(t)\right) \tag{6}$$

over a range of steady-state monitor responses, m_{ss}. Note that the upper-limit for this range need not exceed the maximum m_{ss} for all deformations.

2) Solve for the protection level probability (P_{pl}) constant, K_{pl}, using

$$K_{pl}=\left(\Phi^{R}\right)^{-1}\left(P_{pl,max}\right)=\left(\Phi^{R}\right)^{-1}\left(\frac{P_a}{P_{md}(m(t))P_f}\right) \tag{7}$$

3) Solve for the bound on $E(t)$ using Equation A-7. (Note that this bound depends on the UDRE.)

4) Divide this bound by the step response in Eq. A-14 and take the minimum over all time to yield the minimum E_{ss} vs. m_{ss} curve, or the "time-varying MERR" curve.

5) Compute the scale factors, S, required to reduce the monitor noise and thereby ensure the MERR curve bounds all threats according to Equation 8. Note that for L1-only users, these are pre-determined; a different curve applies to each UDREI. Using these established factors we can set the minimum performance level (i.e., MERR bounds) of the existing monitor. Any proposed monitor design should meet these requirements to be valid.

$$S=\min_{S_0}\left\{\left|E(t)\right|\le MERR\left(\frac{P_a}{P_{md}(m(t)\cdot S_0)P_f}\right)\right\} \tag{8}$$

Figure 11 plots the MERR limits for each UDRE in addition to the same E_{ss} vs. m_{ss} upper bound from Figure 10. These are the minimum monitor responses required to meet the time-to-alert requirement at each UDREI. The MERR curves (i.e., the dashed black lines) are never crossed by the maximum user error curve; they successfully bound the E_{ss} vs. m_{ss} curves whenever all the points lie to the right and/or below them. This implies the current system meets the requirement. Note, however, that even for the smallest error limit, the MERR is always greater than (approximately) 4 meters. This is because for L1-only users, the ionosphere error terms are included in the MERR computation.

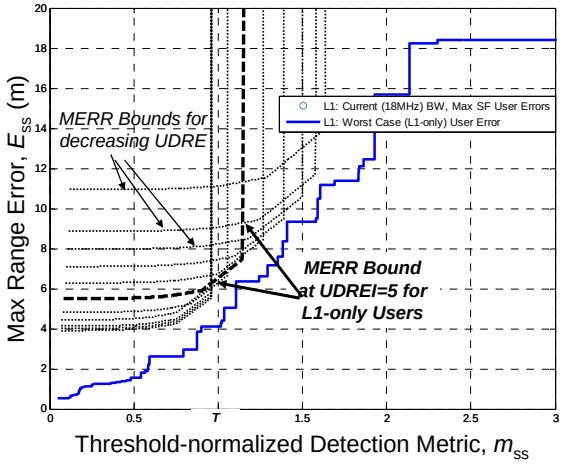

Figure 11. E_{ss} vs. m_{ss} for the current WAAS system for L1-only users. (Reference 18MHz, 0.1 chip) MERR bounds for each UDRE are shown (black, dashed).

As previously stated, for the monitor analysis of this paper, it was necessary to compute new thresholds (using the NovAtel OEM-V3 receiver) for each monitor design change. This provides a common basis with which to compare their relative performance. Figure 12 plots two L1-only E_{ss} vs. m_{ss} curves—one where the monitor m_{ss} has been normalized using the current WAAS thresholds (from Figures 10 and 11) and one where m_{ss} has been normalized using the OEM-V3 evaluation thresholds. It can be seen that the latter thresholds are significantly more conservative than those used in the current WAAS signal deformation monitor.

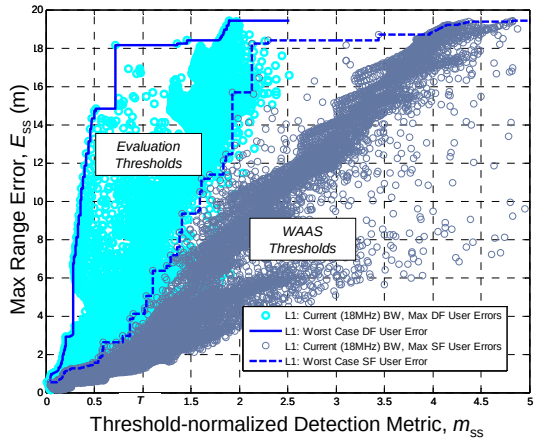

Figure 12. E_{ss} vs. m_{ss} for the current WAAS system for L1-only users (Reference G-II: 18MHz, 0.1 chip) compared to the E_{ss} vs. m_{ss} computed using new, evaluation (OEM-V3 receiver) thresholds.

Figure 12 once again plots the (threshold-adjusted) E_{ss} vs. m_{ss} curve corresponding to L1-only users. This figure also overlays the time-varying MERR bounds for dual-frequency users. Note that here the MERR curve (at the smallest UDREI) descends nearly to zero. And the MERR bound at UDREI=5 is now less than 2.5m since it does not include any ionospheric error terms.

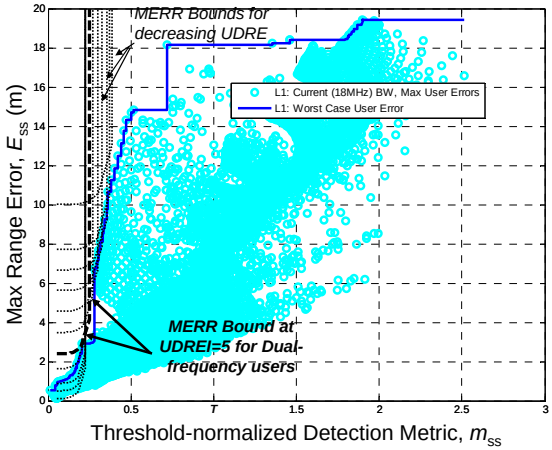

Figure 12. E_{ss} vs. m_{ss} for the current WAAS system for L1-only users (Reference G-II: 18MHz, 0.1 chip) using new, evaluation (OEM-V3 receiver). MERR bounds at each UDRE shown (black, dashed) for dual-frequency users.

RESULTS

Using all the aforementioned inputs, tools, and analysis techniques the following monitor and fault cases were compared:

- L1-only users and a monitor receiver using current G-II (18MHz) receiver and Current WAAS correlator-based metric. This is the baseline case previously discussed. User errors are not scaled. (Refer to Figures 10 and 11.)
- Dual-frequency Users and a SDM using the new G-III (24MHz) receiver with the Current WAAS correlator-based detection metric. The fault occurs only on L1. User errors on each signal are scaled by 2.26.
- Dual-frequency Users and a SDM using the new G-III (24MHz) receiver with the new chip shape-based detection metric. The fault occurs only on L1. User errors are scaled by 2.26.
- Dual-frequency Users and a SDM using the new G-III (24MHz) receiver with the new chip shape-based detection metric. The fault occurs only on L5. User errors are scaled by 1.26.
- Dual-frequency Users and a SDM using the new G-III (24MHz) receiver with the new chip shape-based detection metric. The worst-case fault occurs simultaneously on both L1 and L5. User errors from

threats on each signal are scaled by 2.26 and 1.26 (respectively) then summed.

The results of each of cases are plotted in Figure 13. It can be seen that, for dual-frequency users, just the addition of the wider bandwidth receiver (dark green line) adds a little detection capability over the baseline case (blue line) in some instances. However, the larger user errors from the bandwidth difference and the dual-frequency scaling easily negate this advantage for almost all threat cases.

The introduction of the chip-based detection metric (the red line), however, produces a significant advantage over the previous techniques. The increased detection sensitivity over the current correlator-based techniques is evident. Even the scaling of the errors by 2.26 is manageable for the majority if threat cases. This advantage holds up for both the L5-faulted case and the simultaneous L1, L5 fault case as well.

Figure 14 shows a zoomed in view of Figure 13. In addition, it plots the MERR bounds for dual-frequency users. It can be seen that, given the conservative assumptions of this analysis and no additional considerations, the chip-based metric could, enable a minimum UDREI 4 for dual-frequency users. To enable a smaller UDRE, additional measures would likely need to be taken to reduce the maximum errors.

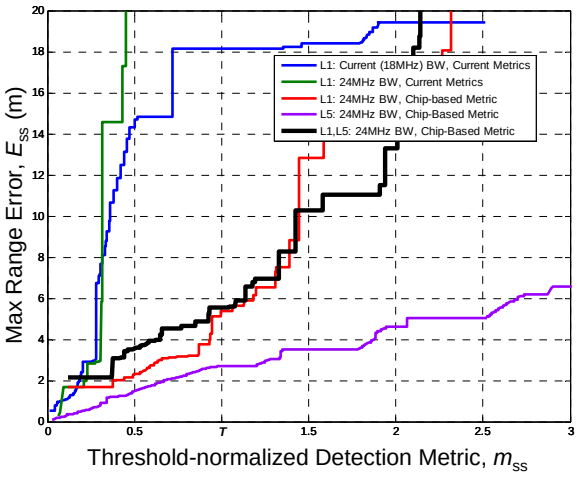

Figure 13. Relative effectiveness of designs for dual-frequency users (as compared to the current WAAS monitor for L1-only users).

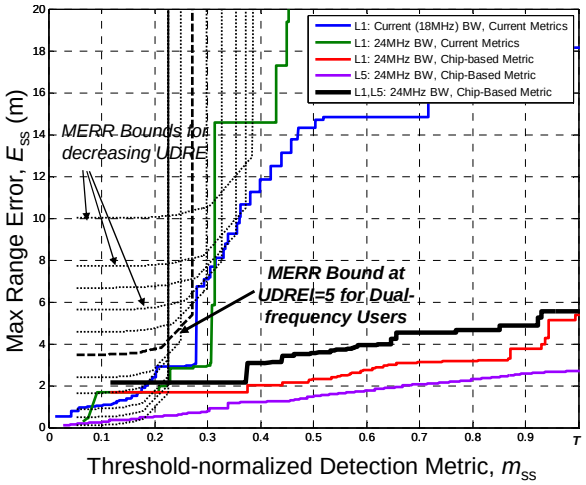

Figure 14. Relative effectiveness of designs for dual-frequency users (as compared to the current WAAS monitor for L1-only users). MERR bounds overlaid for comparison.

All of the previous analyses considered the case when the fault is differentially corrected by the reference receiver. However, a more insidious fault condition exists where the differential correction cannot be applied. In this case, the magnitudes of the user errors are even larger.

To meet this challenge, WAAS uses another monitor in conjunction with the SDM to mitigate the threat within the time-to-alert. The WAAS code-carrier coherence (CCC) monitor is capable of assisting the SDM when this type of signal deformation fault occurs [11]. The details of this monitor and its MERR analyses are beyond the scope of this paper. However, presuming this monitor is in place, we can assess the ability of the SDM to effectively mitigate the remaining, un-corrected faults in the same way we have before.

The results of the uncorrected fault case are shown in Figure 15. Here, meeting the simultaneous L1-L5 fault case (heavy, solid black line) for dual frequency users is significantly more challenging than most of the other monitoring cases. However, the plot still shows that the chip-based monitoring detection metric still nearly enables the system to a minimum UDREI of 4. It also outperforms the current metric which would be incapable of mitigating the threats with such large errors and is not designed to mitigate threats on L5.

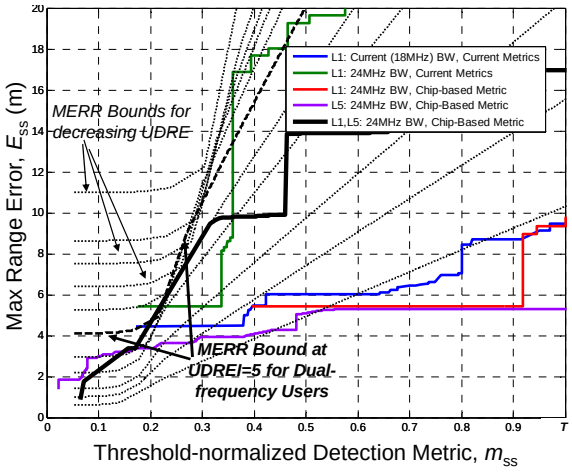

Figure 15. Relative effectiveness of monitor designs for dual-frequency users (as compared to the current WAAS monitor for L1-only users) with *no differential correction applied*. MERR bounds shown for comparison.

Conservative Measures

The results presented here are somewhat pessimistic for several reasons. For one, the dual-frequency threat model is more conservative here than will be assumed in practice. The analysis used here presumed an independent fault on each signal that was additive. In reality, WAAS will assert that only a single fault can affect both signals simultaneously; this will result in some cancellation of the biases in the dual-frequency combination equation. The worst case bias magnitude will then become the case of a signal fault on L1 only.

A second pessimistic assumption was that the dual-frequency WAAS avionics receivers will have nearly the same design latitude as do current L1-only users. In reality, proposals are already in the works to limit the constraint space to the vicinity of the ground reference receiver. While it is not certain that such a proposal will be finalized, it is clear that the configurations will be far more limited than those analyzed here. This will further reduce the maximum errors experienced by dual-frequency users

Finally, none of these results include the benefits for single-frequency users. The new receivers and metrics will likely be in place serving L1-only WAAS users long before there are sufficient L5 signals on orbit to serve the needs of dual-frequency users. However, benefits for single frequency users should not be dismissed. The chip-based detection metric effectiveness curves for single-frequency users reduce to the L1-only case (the red curves of in Figures 13, 14, and 15), without the dual-frequency amplification factor of 2.26. This effectively means the smallest error limits (UDREI=0) could be enabled for single-frequency users. Alternatively, the current performance could be met using much larger monitor thresholds, thereby further reducing the probability of false alarms.

CONCLUSION

In this paper the challenge of mitigating signal deformation faults for dual-frequency WAAS users is discussed. To this end, a new detection metric was proposed based on the capabilities of the new WAAS receiver which has a wide (24MHz) bandwidth and provides outputs of the code chip shape. While the bandwidth slightly increases detection performance, the chip-based measurements are more sensitive than traditional correlation peak-based ones mainly because they avoid the correlation process, which tends to average out some of the distortion effects.

It is shown that the new metric is easily applied to the L5 signal in addition to L1 and is sensitive enough to detect the threats far better than the existing WAAS SDM algorithm. While the existing error limit is currently 6.08m for L1-only users, the addition of the new 24MHz monitor receivers, combined with the new metric, should permit an error limit as small as 3.64 meters for dual-frequency users.

The detection performance results presented are likely more pessimistic here than they would be in the WAAS system for the following reasons:

- The two-frequency fault case—a simultaneous fault occurring on both signals of the same satellite—was significantly more conservative in this analysis than will ultimately be asserted. While additive errors were modeled here, a notable degree of error cancellation is expected for that scenario.
- The allowed receiver configurations will likely be constrained to those designs more akin to the ground receiver, significantly reducing the worst case user errors
- Benefits to L1-only users are perhaps as important as those for dual-frequency users. Significant reductions in the minimum achievable UDRE and/or increases to the SDM detection thresholds may be possible with this new hardware and detection method. This, in combination with other system improvements may lead to improved availability for single frequency users [12].

APPENDIX A: Derivation of the Time-Varying MERR

This section develops a mathematical formulation for the time-varying Maximum allowable ERror in Range (MERR) for signal deformation biases. For a more-complete description including additional background concerning relationship to the "static MERR" concept as used in the Phase I WAAS SV19/CCC monitor analysis [11], refer to [9].

If the fault-induced ranging error exceeds the MERR bound at any time, SBAS integrity cannot be ensured. For a system anomaly to result in a hazardous error, two simultaneous failures must occur. First, ground monitoring must fail to detect the anomaly, and second, the protection level (PL) must fail to bound the resulting navigation error. The MERR will be defined to reflect the conditional risks associated with this

$$\frac{P_a}{P_f} \geq P_{pl}(t) P_{md}(t) \tag{A-1}$$

This MERR formulation recognizes than both the probability of exceeding the VPL $P_{pl}(t)$ and the probability of detecting the fault Pmd(t) are both functions of time. P_a/P_f is a constant. It is the ratio of the fault tree allocation (P_a) for the monitor to the prior probability (P_f) of the fault.

The equation for $P_{md}(t)$ is given by

$$P_{md}(t - RDT) = \left(\Phi^R\right)\left(\frac{T - m(t)}{\sigma_{mon}}\right) - \left(\Phi^R\right)\left(\frac{-T - m(t)}{\sigma_{mon}}\right) \tag{A-2}$$

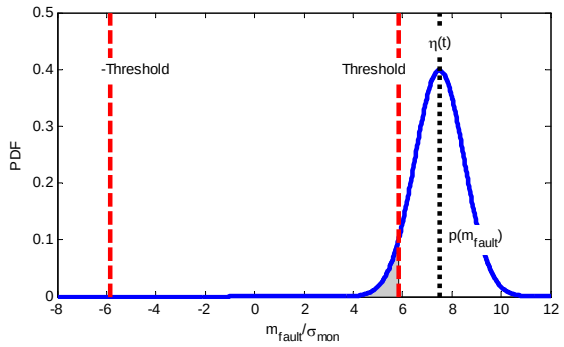

Figure A-1. Monitor P_{md} evaluation.

To address the time-to-alert requirement, in the above equation we have defined a term, RDT to indicate the Relative Time-to-Detect. The warning from the ground system must reach the user in a timely fashion. The required time between the onset of a hazardous condition and the arrival of the warning message at the user is called Time-to-Alert (TTA). The actual worst case Time-to-Transmit (TTT) the warning message may be longer or shorter than the required TTA. If transmission time is longer than the specified TTA, the monitor must make up the difference by triggering early. If the transmission time is shorter than the allowed alert time, then the monitor may trigger late, after the fault becomes hazardous. In either case, the time difference is referred to as the Relative Detection Time (RDT). RDT = TTA−TTT. For WAAS, RDT = 0.

The probability that the fault exceeds the protection level is given by

$$P_{pl} \leq \left(\Phi^R\right)\left(\frac{-VPL + \left|S_{v,i} E(t)\right|}{\sqrt{\sum_i S_{v,i}^2 \sigma_{UDREI\_nom,i}^2}}\right) \tag{A-3}$$

In the above equation, VPL is the desired vertical protection level. $E(t)$ is the time-varying user range error. $S_{v,i}$ are the sensitivity weights that transform the range error into the vertical direction. $\sigma^2_{UDREI\_nom,i}$ is the variance on the ith ranging signal.

In the vertical direction (for the ith satellite),

$$VPL = K_{ffd} \sqrt{\sum_i S_{v,i}^2 \sigma_{tot,i}^2} \tag{A-4}$$

where σtot,i is the MERR values tabulated in Table 3 (divided by 5.33) as a function of UDREI. The error seen by the user is given by the sum of the bias component and the random component according to

$$Vertical\ Position\ Error = \left|S_{v,i}\right|\left|E(t)\right| + K_{pl} \sqrt{\sum_i S_{v,i}^2 \sigma_{UDRE\_nom,i}^2} \tag{A-5}$$

The protection level is not exceeded provided the following holds

$$\left|S_{v,i}\right|\left|E\right| \leq K_{ffd} \sqrt{\sum_i S_{v,i}^2 \sigma_{tot,i}^2} - K_{pl} \sqrt{\sum_i S_{v,i}^2 \sigma_{UDREI\_nom,i}^2} \tag{A-6}$$

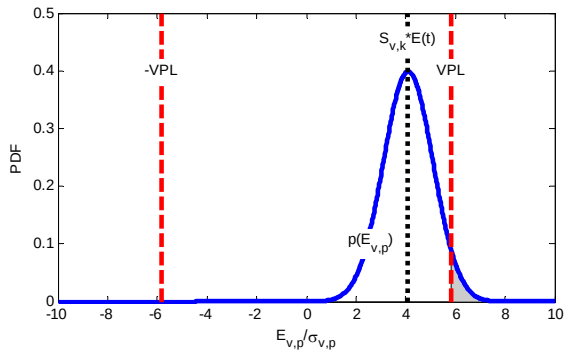

Figure A-2. Monitor P_{pl} evaluation

In the above equation, K_{ffd} is the constant multiplier required to meet the continuity (i.e., false alarm) requirement. After simplifying the above equations, the bound on the error $E(t)$ becomes

$$\left|E(t)\right| \le \left(K_{ffd}\sigma_{tot,i} - K_{pl}\sigma_{UDRE\_nom,i}\right) \quad \text{(A-7)}$$

Where

$$\sigma_{tot,i} = \sqrt{\sigma_{UDRE}^2 + \left(F_{PP}\sigma_{UIRE}\right)^2} \quad \text{(A-8)}$$

The probability of exceeding the protection level (i.e., the error bound in range domain) is then

$$P_{pl} \le \left(\Phi^R\right)\left(\frac{\sigma_{tot,i}}{\sigma_{UDRE\_nom,i}}\left(\left|E(t)\right| - K_{ffd}\right)\right), \quad \text{(A-9)}$$

and the integrity test in risk form is given by

$$\frac{P_a}{P_f} \ge P_{pl}\left(E(t)\right)\cdot P_{md}\left(m(t)\right) \quad \text{(A-10)}$$

In the above equation, E(t) is the time-varying user range error and $m(t)$ is the time-varying monitor response. The integrity test in "MERR form" becomes

$$\left|E(t)\right| \le MERR\left(P_{pl,max}(t)\right) \quad \text{(A-11)}$$

where

$$P_{pl,\max} = \frac{P_a}{P_{md}\left(m(t)\right)P_f}, \quad \text{(A-12)}$$

and $P_{pl,\max}$ is the maximum probability of exceeding the protection level. This MERR is a line that bounds the Maximum User Error E_{ss} as a function of the Maximum Monitor Statistic m_{ss}.

The first-order filtered, monitor response m(t), normalized by its steady-state value for each signal deformation in the threat model mss is given by a unit step response of the correlator metrics with Gaussian statistics.

$$\frac{m(t)}{m_{ss}} = \left(1 - e^{-t/\tau_{mon}}\right) \quad \text{(A-13)}$$

In the above equation, τ_{mon} is the nominal time constant for the monitor metric smoothing filter.

The first-order filtered, user error $E(t)$ normalized by its steady-state value for each signal deformation in the threat model E_{ss} is given by a unit step response of the code range error metrics with Gaussian statistics.

$$\frac{E(t)}{E_{ss}} = \left(1 - e^{-t/\tau_{csc}}\right) \quad \text{(A-14)}$$

In the above equation, τ_{csc} is the nominal time constant for the user carrier smoothing filter.

The probability of hazardous misleading information (P_{HMI}) due to undetectable signal deformation range biases is found directly from satisfying the above equations. It takes into account nominal correction errors (satellite clock and ephemeris, ionosphere) present in the system, and is accordingly equal to the fault tree allocation. A simple procedure for computing the time-varying MERR curve for SQM is outlined in the Analysis section.

ACKNOWLEDGEMENTS

This work was sponsored by the FAA GPS Satellite Product Team (AND-730).

REFERENCES

[1] Liu, F., Brenner, M., Tang, C.Y., "Signal Deformation Monitoring Scheme Implemented in a Prototype Local Area Augmentation System Ground Installation," *Proceedings of the 19th International Technical Meeting of the Satellite Division of the Institute of Navigation*, ION GNSS-2006, September 2006.

[2] Phelts, R.E., (2001) *Multicorrelator Techniques for Robust Mitigation of Threats to GPS Signal Quality*, Ph.D. Thesis, Stanford University, Stanford, CA.

[3] Phelts, R. E., Walter, T., Enge, P., "Toward Real-Time SQM for WAAS: Improved Detection

Techniques," *Proceedings of the 16th International Technical Meeting of the Satellite Division of the Institute of Navigation*, ION GPS/GNSS-2003, September 2003.

[4] "International Standards and Recommended Practices," *Aeronautical Telecommunications*, ICAO, Vol. 1, Annex 10, July 2006.

[5] Phelts, R. E., Akos, D. M., "Effects of Signal Deformations on Modernized GNSS Signals," *Journal of Global Positioning Systems,* Vol. 5 No. 1-2, Hong Kong, China, 2006.

[6] Minimum Operational Performance Standards (MOPS) for WAAS, DO-229D. *RTCA*.

[7] Fenton, P., Jones J., ., "The Theory and Performance of NovAtel Inc.'s Vision Correlator," *Proceedings of the 19th International Technical Meeting of the Satellite Division of the Institute of Navigation*, ION GNSS-2006, September 2006

[8] Wong, G., Phelts, R.E., Walter, T., Enge, P., "Alternative Characterization of Analog Signal Deformation for GPS Satellites", International Technical Meeting of the Institute of Navigation, January, 2011.

[9] Rife, J., Phelts, R. E., "Formulation of a Time-Varying Maximum Allowable Error for Ground-Based Augmentation Systems," National Technical Meeting of the Institute of Navigation, January 18-20, 2006.

[10] Hsu, P., Chiu, T., Golubev, Y., Phelts, R. E., "Test Results for the WAAS Signal Quality Monitor," *Proceedings of Position Location and Navigation Symposium*, IEEE/ION PLANS, 2008.

[11] Shloss, P., Phelts, R. E., Walter, T., Enge, P., "A Simple Method of Signal Quality Monitoring for WAAS LNAV/VNAV," *Proceedings of the 15th International Technical Meeting of the Satellite Division of the Institute of Navigation*, ION GPS/GNSS-2002, September 2002.

[12] Blanch, J., Phelts, R.E., Walter, T., Enge, Per, "Near Term Improvements to WAAS Availability," International Technical Meeting of the Institute of Navigation, January 28-30, 2013.